European Radiology (2019) 29:1425–1434
https://doi.org/10.1007/s00330-018-5667-9

MAGNETIC RESONANCE

# Added value of mean and entropy of apparent diffusion coefficient values for evaluating histologic phenotypes of invasive ductal breast cancer with MR imaging

Shiteng Suo[1] · Dandan Zhang[1] · Fang Cheng[1] · Mengqiu Cao[1] · Jia Hua[1] · Jinsong Lu[2] · Jianrong Xu[1]

Received: 8 May 2018 / Revised: 19 June 2018 / Accepted: 13 July 2018 / Published online: 16 August 2018


## Abstract

**Objectives** To study the added value of mean and entropy of apparent diffusion coefficient (ADC) values at standard (800 s/mm$^2$) and high (1500 s/mm$^2$) *b*-values obtained with diffusion-weighted imaging in identifying histologic phenotypes of invasive ductal breast cancer (IDC) with MR imaging.

**Methods** One hundred thirty-four IDC patients underwent diffusion-weighted imaging with *b*-values of 800 and 1500 s/mm$^2$, and corresponding $ADC_{800}$ and $ADC_{1500}$ maps were generated. Mean and entropy of volumetric ADC values were compared with molecular markers (estrogen receptor [ER], progesterone receptor [PR], human epidermal growth factor receptor 2 [HER2], and Ki-67). Associations among morphologic features, ADC metrics, and phenotypes (luminal A, luminal B [HER2 negative], luminal B [HER2 positive], HER2 positive, and triple negative) were evaluated.

**Results** Mean ADC values were significantly decreased in ER-positive, PR-positive, and HER2-negative tumors ($p < 0.01$). Ki-67 ≥ 20% tumors demonstrated significantly higher ADC entropy values compared with Ki-67 < 20% tumors ($p < 0.001$). Luminal A subtype tended to display lower ADC entropy values compared with other subtypes, while HER2-positive subtype tended to display higher mean ADC values. $ADC_{1500}$ entropy provided superior diagnostic performance over $ADC_{800}$ entropy ($p = 0.04$). Independent risk factors were $ADC_{1500}$ entropy ($p = 0.002$) associated with luminal A, irregular mass shape ($p = 0.018$) and $ADC_{1500}$ entropy ($p = 0.022$) with luminal B (HER2 positive), mean $ADC_{1500}$ ($p = 0.018$) with HER2 positive, and smooth mass margin ($p = 0.012$) and rim enhancement ($p = 0.003$) with triple negative.

**Conclusions** Mean and entropy of ADC values provided complementary information and added value for evaluating IDC histologic phenotypes. High-*b*-value $ADC_{1500}$ may facilitate better phenotype discrimination.

**Key Points**

- *ADC metrics are associated with molecular marker status in IDC.*
- *$ADC_{1500}$ improves differentiation of histologic phenotypes compared with $ADC_{800}$.*
- *ADC metrics add value to morphologic features in IDC phenotyping.*

**Keywords** Diffusion magnetic resonance imaging · Breast cancer · Phenotype · Immunohistochemistry · Prognosis

Shiteng Suo and Dandan Zhang contributed equally to this work.

**Electronic supplementary material** The online version of this article (https://doi.org/10.1007/s00330-018-5667-9) contains supplementary material, which is available to authorized users.

✉ Jia Hua
huajia_renji@163.com

✉ Jianrong Xu
xujianrong_renji@163.com

[1] Department of Radiology, Renji Hospital, School of Medicine, Shanghai Jiao Tong University, No. 160, Pujian Rd, Shanghai 200127, China

[2] Department of Breast Surgery, Renji Hospital, School of Medicine, Shanghai Jiao Tong University, Shanghai, China

**Abbreviations**

| | |
|---|---|
| ADC | Apparent diffusion coefficient |
| DCE | Dynamic contrast enhanced |
| DWI | Diffusion-weighted imaging |
| ER | Estrogen receptor |
| HER2 | Human epidermal growth factor receptor 2 |
| IDC | Invasive ductal carcinoma |
| IHC | Immunohistochemistry |
| OR | Odds ratio |
| PR | Progesterone receptor |
| ROC | Receiver-operating characteristic |
| ROI | Region of interest |
| SPAIR | Spectral adiabatic inversion recovery |
| THRIVE | T1-weighted high resolution isotropic volume examination |

## Introduction

Breast cancer is a highly heterogeneous collection of malignancies with different histologic features, clinical manifestations, and responses to treatment. At the genetic level, breast cancers are generally classified into four intrinsic molecular phenotypes: luminal A, luminal B, human epidermal growth factor receptor 2 (HER2) enriched, and basal like [1]. Clinical identification of different phenotypes is routinely obtained by immunohistochemistry (IHC) of several molecular markers including the estrogen receptor (ER), progesterone receptor (PR), HER2, and Ki-67 labeling index [2]. Preoperative phenotyping of breast cancer is essential because it may predict neoadjuvant chemotherapy responsiveness and allow optimized strategies for patient-tailored therapy.

Core biopsy has already been established as a valid method for the diagnosis of suspicious breast cancer and investigation of molecular markers. However, biopsy samples suffer from limited tumor volumes that cannot represent the full picture of tumor heterogeneity, raising the risk of underestimating the most aggressive component of cancer [3]. Thus, there is an increasing awareness of the importance of using noninvasive imaging techniques to fully capture whole-tumor characteristics [4].

Diffusion-weighted imaging (DWI) is a promising magnetic resonance imaging tool for breast cancer that probes the Brownian motion of water molecules within tissues. Apparent diffusion coefficient (ADC) is a quantitative parameter calculated from DWI and reflects tumor biologic and microstructural features such as cellularity. Although several studies have been performed to investigate the relationships between ADC and molecular markers of breast cancer, the yielded results were inconsistent. For example, a recently published study showed that mean ADC values were significantly lower in HER2-positive invasive breast cancer compared with the HER2-negative group [5], whereas most studies reported the opposite [6, 7] or no significant difference [8–10]. Several image-related factors may account for these conflicting findings such as use of different maximal *b*-values (standard vs. high) and region-of-interest (ROI) placement methods (single-section vs. whole-tumor). There has been considerable effort to use ADC volumetric analysis encompassing the whole tumor, which would potentially eliminate sampling bias [4]. In addition, volumetric image analysis can provide surrogate markers of overall tumor heterogeneity with histograms [11]. Entropy is an indicator of tumor heterogeneity by depicting the variation in ADC volumetric histograms and has been shown to be useful to differentiate benign from malignant breast lesions [12]. Limited literature exists on the utility of ADC entropy in evaluation of prognostic factors and histologic phenotypes in invasive breast cancer [13].

Thus, the aim of this study was to explore the added value of mean and entropy of ADC obtained at standard- and high-*b*-value (800 and 1500 s/mm$^2$, respectively) DWI in identifying histologic phenotypes in invasive ductal breast cancer.

## Materials and Methods

### Patients

This retrospective study was approved by the institutional review board, and the need for informed patient consent was waived. Between July 2015 and May 2017, 393 patients diagnosed at biopsy histologically with breast malignancies underwent preoperative 3.0-T breast MR imaging and subsequently received mastectomy or lumpectomy. To eliminate the effects of MR imaging parameter and breast cancer histologic type on the results, we included only patients with invasive ductal carcinoma (IDC) scanned on the same MR imaging platform with a unified imaging protocol ($n$ = 206). We excluded the following patients: (1) those treated with neoadjuvant chemotherapy ($n$ = 58), (2) those with lesions that were scarcely identified on DWI ($n$ = 12, tumor size < 10 mm), or (3) those for which DWI was adversely influenced by motion artifacts ($n$ = 2). For patients with multiple invasive ductal carcinomas, only the largest lesion was used for statistical analysis. Thus, 134 female patients (mean age, 51.6 years; range, 26–84 years) with 134 lesions were included.

### MR Imaging Protocol

MR imaging was performed by using a 3-T system (Ingenia, Philips Medical Systems). All patients were placed in the prone position with both breasts suspended into the dedicated bilateral, four-channel, phased-array breast coil. We performed the DWI with a single-shot spin-echo echo-planar imaging sequence in three

orthogonal directions by using the following parameters: repetition time/echo time, 4500/85 ms; field of view, 280 × 340 mm$^2$; matrix, 108 × 128; section thickness, 3 mm; *b*-values, 0, 800, and 1500 s/mm$^2$; number of excitations, 3. Fat suppression was attained with a chemically selective spectral adiabatic inversion recovery (SPAIR) technique. Parallel imaging was incorporated with an acceleration factor of 2. Other MR acquisitions are detailed in the Supplemental Material 1.

## Image Analysis

For qualitative morphologic analysis, MR images were reviewed in consensus by two radiologists with more than 17 and 8 years of experience in breast MR imaging interpretation, without knowledge of the histopathologic results. Morphologic features (mass or non-mass; shape, margin, and internal enhancement in the mass lesion; distribution and internal enhancement in the non-mass lesion) and kinetic curve patterns (persistent, plateau, or washout) were assessed based on dynamic contrast-enhanced (DCE) MR images by using the Breast Imaging Reporting and Data System MR lexicon [14]. Additionally, the intratumoral signal intensity was visually evaluated on fat-suppressed T2-weighted MR images and categorized as low, equal, or high compared with the surrounding parenchymal signal intensity [15, 16].

For quantitative ADC analysis, all patient image raw data were transferred to an independent personal computer. Image processing was performed with a custom-made algorithm developed in a numerical computing environment and programming language (MATLAB version 2016a, MathWorks). Diffusion-weighted images were first loaded into the software, and ADC values were calculated by using diffusion-weighted images with a *b*-value of 0 and a second nonzero *b*-value, according to the equation: $ADC = (-1/b) \times \ln(S_b/S_0)$, where *b* is the *b*-value (s/mm$^2$) and $S_b$ and $S_0$ the signal intensity with and without diffusion gradient, respectively. In this study, we used standard and high *b*-values of 800 and 1500 s/mm$^2$ respectively, to generate $ADC_{800}$ and $ADC_{1500}$ maps. ROIs that encompassed the entire tumor were manually drawn on all corresponding sections of $ADC_{800}$ maps and copied to $ADC_{1500}$ maps (Fig. 1). Tumor boundaries were defined with reference to the DCE MR imaging data by the aforementioned radiologist with more than 8 years of experience in breast MR imaging interpretation. Meanwhile, cystic or necrotic areas were excluded by visual judgment. For each case, the mean ADC value of the tumor was calculated as the average across all pixels within the selected ROIs. Histogram-based entropy was determined on the ADC histogram as a statistical measure representing the irregularity of pixel value distribution [17]. Higher entropy values indicate higher heterogeneity [18]. Entropy was computed as follows: $\text{entropy} = \sum(-p_i)\log(p_i)$, where $p_i$ is the frequency of ADC values in the ROIs and defined as normalization of the pixel number of the specific ADC value to the total pixel number.

## Histopathologic Assessment

Surgical specimens were used for histopathologic assessment. Molecular marker statuses (ER, PR, HER2, and Ki-67) were determined by IHC or a combination of IHC and *in situ* hybridization assays. ER or PR positivity was defined as ≥ 1% nuclear immunostaining. HER2 expression was evaluated as positive when membrane immunostaining was scored 3+ or when HER2 gene amplification was demonstrated by *in situ* hybridization assays in case of a 2+ score by IHC. The Ki-67 index was assessed as the percentage of immunoreactive tumor cells, and a cut-off value of 20% was used to define the low- and high-proliferation tumor groups [19]. The histologic phenotypes of IDC were categorized as luminal A, luminal B

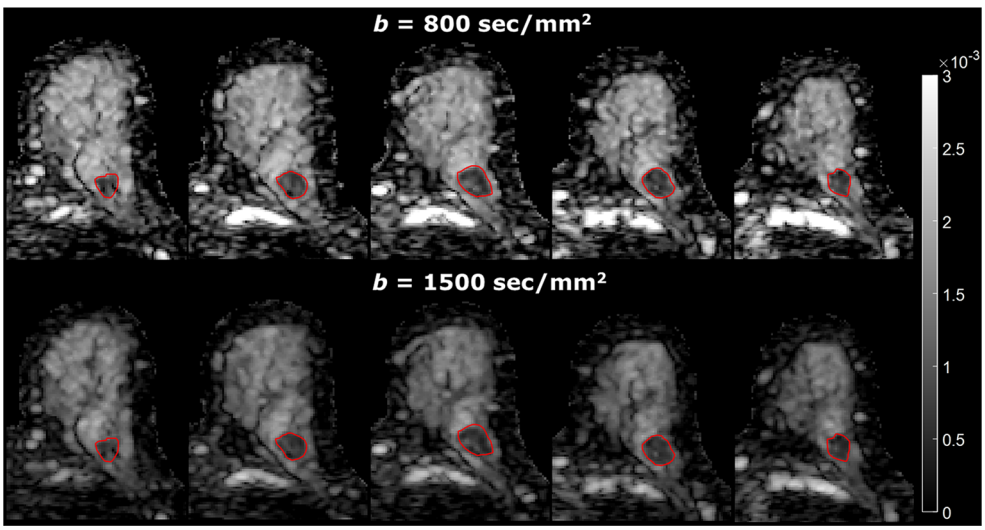


**Fig. 1** ADC maps obtained at *b* = 800 s/mm$^2$ and *b* = 1500 s/mm$^2$ in a 45-year-old female with luminal B (HER2-negative) invasive ductal carcinoma show ROI placement methods. Freehand ROIs on all sections containing the tumor are included to generate the volumetric data for analysis

(HER2 negative), luminal B (HER2 positive), HER2 positive, and triple negative.

## Statistical Analysis

All continuous variables were reported as means ± standard deviations, and categorical variables were reported as numbers and percentages. The Shapiro-Wilk test and Leven test were first used to analyze the normality and homoscedasticity of quantitative measurements, respectively. The possible associations between mean and entropy of ADC values and molecular marker statuses (ER, PR, HER2, and Ki-67) were assessed by using the independent Student *t* test for normally distributed variables and the Mann-Whitney *U* test for non-normally distributed variables. The MR imaging morphologic features were compared among histologic phenotypes by using the $\chi^2$ or Fisher's exact tests. For comparison of ADC data differences in histologic phenotypes, the one-way analysis of variance was used for normally distributed variables and the Kruskal-Wallis nonparametric test for non-normally distributed variables. Significant results were subject to the post hoc Tukey test and Dunn test for parametric and nonparametric analysis, respectively, to identify individual differences between groups. The diagnostic effectiveness of mean and entropy of ADC values in differentiating one specific phenotype from other phenotypes was evaluated by using receiver-operating characteristic (ROC) analysis. The optimal threshold was determined by maximizing the Youden index. Areas under the ROC curves were compared by using the method developed by DeLong et al [20]. A leave-one-out cross-validation approach was used to evaluate the performance of the independent variables, and sensitivity and specificity were calculated accordingly. Univariate and multivariate logistic regression analyses were performed to screen the independent risk factors associated with one specific phenotype. Variables with a $p$ value < 0.05 at univariate analysis were entered into multivariate backward stepwise logistic regression analysis.

$P < 0.05$ was considered to indicate a statistical significance. Statistical analyses were carried out using SPSS version 20 (IBM Corp.) and Prism 5 (GraphPad Software Inc.).

## Results

The molecular marker statuses in our study population are summarized in Table 1. Of the tumors, 81 (60.4%) were ER positive, 80 (59.7%) were PR positive, 50 (37.3%) were HER2 positive, and 95 (70.9%) were identified with Ki-67 ≥ 20%. Regarding histologic phenotypes, 27 (20.1%) were luminal A, 36 (26.9%) were luminal B (HER2 negative), 34 (25.4%) were luminal B (HER2 positive), 17 (12.7%) were HER2 positive, and 20 (14.9%) were triple negative.

Mean and entropy ADC values calculated at $b = 800$ s/mm$^2$ were $0.86 \times 10^{-3}$ mm$^2$/s ± 0.15 and 5.43 ± 0.62, respectively; both were significantly higher than those calculated at $b = 1500$ s/mm$^2$ ($0.72 \times 10^{-3}$ mm$^2$/s ± 0.12 and 5.32 ± 0.56, respectively) ($p < 0.001$). Table 1 shows the results of comparisons of mean and entropy of ADC values in multiple subgroups classified according to the molecular marker statuses. ER-negative tumors showed significantly higher mean

**Table 1** ADC parameters according to molecular marker statuses in IDC

| Variables | No. of cases* | $b$ = 800 s/mm$^2$ | | | | $b$ = 1500 s/mm$^2$ | | | |
|---|---|---|---|---|---|---|---|---|---|
| | | Mean ADC† | $p$ value | ADC entropy | $p$ value | Mean ADC† | $p$ value | ADC entropy | $p$ value |
| Estrogen receptor | | | | | | | | | |
| Negative | 53 (39.6) | 0.92 ± 0.15 | < 0.001 | 5.55 ± 0.60 | 0.049 | 0.76 ± 0.12 | < 0.001 | 5.44 ± 0.56 | 0.024 |
| Positive | 81 (60.4) | 0.82 ± 0.14 | | 5.35 ± 0.63 | | 0.69 ± 0.12 | | 5.25 ± 0.56 | |
| Progesterone receptor | | | | | | | | | |
| Negative | 54 (40.3) | 0.92 ± 0.13 | < 0.001 | 5.43 ± 0.60 | 0.976 | 0.76 ± 0.10 | < 0.001 | 5.32 ± 0.56 | 0.858 |
| Positive | 80 (59.7) | 0.82 ± 0.15 | | 5.43 ± 0.64 | | 0.69 ± 0.13 | | 5.32 ± 0.57 | |
| Human epidermal growth factor receptor 2 | | | | | | | | | |
| Negative | 84 (62.7) | 0.84 ± 0.15 | 0.009 | 5.36 ± 0.67 | 0.103 | 0.69 ± 0.12 | 0.008 | 5.25 ± 0.61 | 0.077 |
| Positive | 50 (37.3) | 0.91 ± 0.15 | | 5.56 ± 0.51 | | 0.75 ± 0.12 | | 5.45 ± 0.46 | |
| Ki-67 | | | | | | | | | |
| < 20% | 39 (29.1) | 0.83 ± 0.15 | 0.098 | 4.98 ± 0.58 | < 0.001 | 0.69 ± 0.12 | 0.071 | 4.88 ± 0.51 | <0.001 |
| ≥ 20% | 95 (70.9) | 0.88 ± 0.15 | | 5.62 ± 0.54 | | 0.73 ± 0.12 | | 5.50 ± 0.48 | |

Unless otherwise specified, data are means ± standard deviations

*ADC* apparent diffusion coefficient, *IDC* invasive ductal carcinoma

* Data are numbers with percentages in parentheses

† Data are in units of $\times 10^{-3}$ mm$^2$/s

$ADC_{800}$ or $ADC_{1500}$ values (both $p < 0.001$) and higher $ADC_{800}$ or $ADC_{1500}$ entropy values ($p = 0.049$ and 0.024, respectively) than ER-positive tumors. Likewise, PR-negative tumors showed significantly higher mean $ADC_{800}$ or $ADC_{1500}$ values than PR-positive tumors (both $p < 0.001$). Mean $ADC_{800}$ or $ADC_{1500}$ values were also significantly higher in HER2-positive tumors compared with HER2-negative tumors ($p = 0.009$ and 0.008, respectively). As far as Ki-67 expression, mean ADC values showed no significant difference between Ki-67 ≥ 20% and Ki-67 < 20% groups ($p = 0.098$ and 0.071, respectively). However, Ki-67 ≥20% tumors demonstrated significantly higher $ADC_{800}$ or $ADC_{1500}$ entropy values compared with Ki-67 < 20% tumors (both $p < 0.001$).

Comparisons of ADC metrics in terms of histologic phenotypes are illustrated in Fig. 2. The one-way analysis of variance revealed that mean $ADC_{800}$ or $ADC_{1500}$ values were significantly different among all groups (both $p < 0.001$). The post-hoc test showed that the HER2-positive phenotype represented significantly higher mean $ADC_{800}$ or $ADC_{1500}$ values than luminal A (both $p < 0.001$), luminal B (HER2 negative) (both $p < 0.01$), and luminal B (HER2 positive) (both $p < 0.01$) phenotypes. The Kruskal-Wallis nonparametric test revealed significant difference in $ADC_{800}$ or $ADC_{1500}$ entropy values among all groups (both $p < 0.001$). Luminal A phenotype seemed to demonstrate lower $ADC_{800}$ or $ADC_{1500}$ entropy values than other phenotypes, and the post-hoc test showed that, for $ADC_{800}$, this difference was significant between luminal A and other phenotypes (all $p < 0.05$) except HER2 positive ($p > 0.05$), and for $ADC_{1500}$, this difference was significant between luminal A and each other phenotype (all $p < 0.05$). Representative $ADC_{800}$ and $ADC_{1500}$ maps with histograms for HER2-positive and luminal A phenotypes are illustrated in Figs. 3 and 4.

Morphologic features at MR imaging stratified by histologic phenotype are shown in Table 2. On DCE MR images, there was no significant difference in morphology (mass or non-mass) or kinetic curve pattern among all groups ($p = 0.462$ and 0.337, respectively). In the 76 mass lesions, significant differences in shape, margin, and internal enhancement among all groups were observed (all $p < 0.05$), while in the 58 non-mass lesions, no significant difference in distribution or internal enhancement was found (both $p > 0.05$). On T2-weighted images, intratumoral signal intensity showed a significant difference among all groups ($p = 0.037$).

Detailed results of ROC analyses are summarized in Table 3. $ADC_{1500}$ entropy showed a significantly larger area under the ROC curve than $ADC_{800}$ entropy (0.830 vs. 0.818, $p = 0.04$) in the differentiation between luminal A and other phenotypes. By using $ADC_{1500}$ entropy as a discriminative index, the respective sensitivity and specificity were 74.1% and 76.6%. To distinguish HER2 positive from other phenotypes, mean $ADC_{1500}$ achieved a similar area under the ROC curve

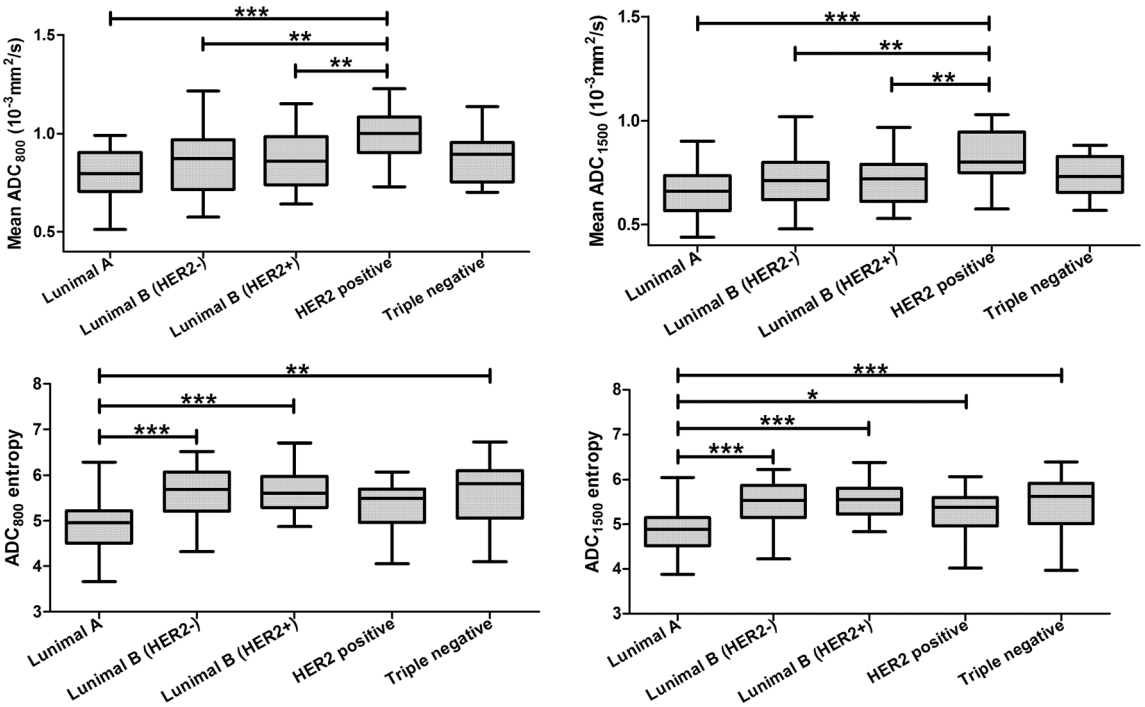


**Fig. 2** Box plots shows mean and entropy ADC values calculated at $b = 800$ s/mm$^2$ and $b = 1500$ s/mm$^2$ for histologic phenotypes of invasive ductal breast cancer. Significant differences in each ADC parameter were observed among all subgroups ($p < 0.05$). *$p < 0.05$, **$p < 0.01$, and ***$p < 0.001$ for post hoc pairwise comparisons

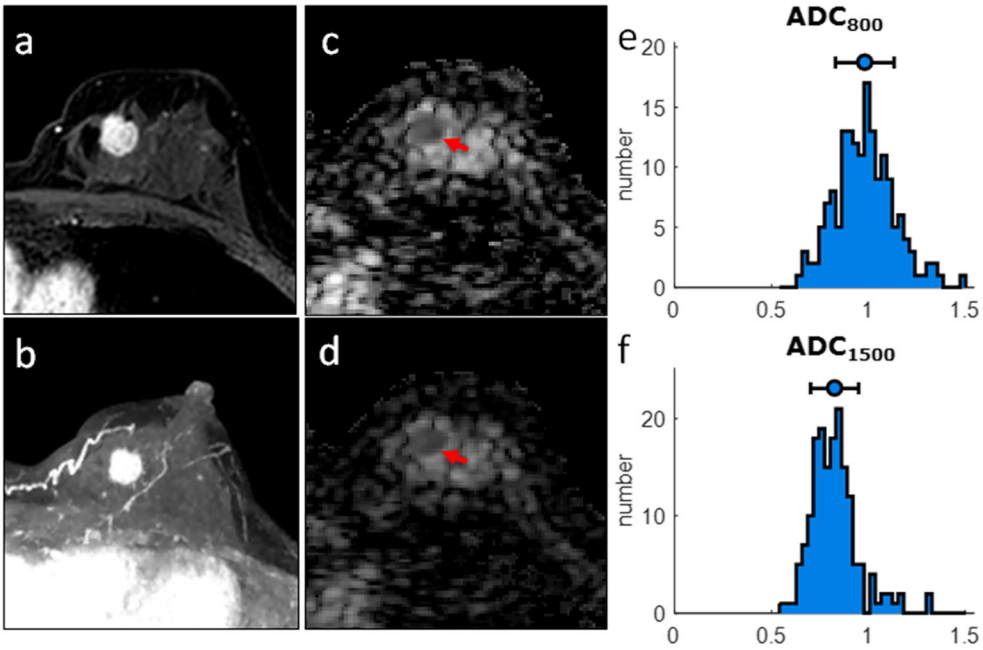


**Fig. 3** Images in a 59-year-old female with HER2-positive invasive ductal carcinoma (Ki-67 index, 40%). **(a, b)** Axial dynamic contrast-enhanced and corresponding maximum intensity projection images show a hyperintense lesion with oval shape and smooth margin. **(c)** $ADC_{800}$ map and **(d)** $ADC_{1500}$ map with corresponding **(e, f)** histograms show decreased ADC values (higher than those of the case in Fig. 4) compared with surrounding parenchyma in the tumor (arrows). Both mean and entropy of ADC values decreased when *b*-value increased from 800 to 1500 s/mm$^2$ ($0.98 \times 10^{-3}$ mm$^2$/s vs. $0.83 \times 10^{-3}$ mm$^2$/s and 4.95 vs. 4.90, respectively). ADC histograms are plotted with ADC values ($\times 10^{-3}$ mm$^2$/s) on the x-axis and with the number of pixels on the y-axis

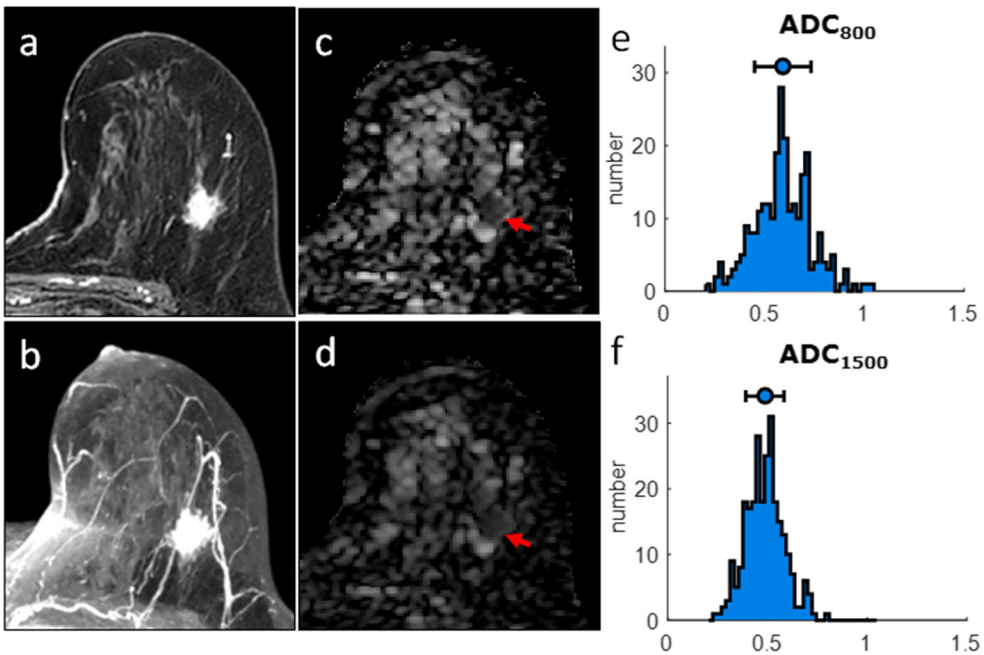


**Fig. 4** Images in a 54-year-old female with luminal A invasive ductal carcinoma (Ki-67 index, 5%). **(a, b)** Axial dynamic contrast-enhanced and corresponding maximum intensity projection images show a hyperintense lesion with a spiculated margin. **(c)** $ADC_{800}$ map and **(d)** $ADC_{1500}$ map with corresponding **(e, f)** histograms show decreased ADC values (mostly below $1\times 10^{-3}$ mm$^2$/s) compared with surrounding parenchyma in the tumor (arrows). Both mean and entropy of ADC values decreased when *b*-value increased from 800 to 1500 s/mm$^2$ ($0.57 \times 10^{-3}$ mm$^2$/s vs. $0.47 \times 10^{-3}$ mm$^2$/s and 4.73 vs. 4.64, respectively). ADC histograms are plotted with ADC values ($\times 10^{-3}$ mm$^2$/s) on the x-axis and with the number of pixels on the y-axis

**Table 2** Morphologic features at MR imaging according to histologic phenotypes in IDC

| | Luminal A | Luminal B (HER2 negative) | Luminal B (HER2 positive) | HER2 positive | Triple negative | *p* value |
|---|---|---|---|---|---|---|
| Mass | 12 (44.4) | 22 (61.1) | 18 (52.9) | 10 (58.8) | 14 (70.0) | 0.462 |
| Non-mass | 15 (55.6) | 14 (38.9) | 16 (47.1) | 7 (41.2) | 6 (30.0) | |
| Mass | | | | | | |
| Shape | | | | | | |
| Round/oval | 4 (33.3) | 6 (27.3) | 1 (5.6) | 6 (60.0) | 8 (57.1) | 0.006 |
| Irregular | 8 (66.7) | 16 (72.7) | 17 (94.4) | 4 (40.0) | 6 (42.9) | |
| Margin | | | | | | |
| Smooth | 3 (25.0) | 2 (9.1) | 0 (0) | 1 (10.0) | 6 (42.9) | 0.032 |
| Irregular | 2 (16.7) | 11 (50.0) | 8 (44.4) | 2 (20.0) | 4 (28.6) | |
| Spiculated | 7 (58.3) | 9 (40.9) | 10 (55.6) | 7 (70.0) | 4 (28.6) | |
| Internal enhancement | | | | | | |
| Heterogeneous | 9 (75.0) | 17 (77.3) | 14 (77.8) | 7 (70.0) | 4 (28.6) | 0.027 |
| Rim | 3 (25.0) | 5 (22.7) | 4 (22.2) | 3 (30.0) | 10 (71.4) | |
| Non-mass | | | | | | |
| Distribution | | | | | | |
| Focal | 5 (33.3) | 3 (21.4) | 3 (18.8) | 1 (14.3) | 3 (50.0) | 0.379 |
| Linear | 0 (0) | 0 (0) | 0 (0) | 2 (28.6) | 0 (0) | |
| Segmental | 4 (26.7) | 2 (14.3) | 2 (12.5) | 1 (14.3) | 0 (0) | |
| Regional | 4 (26.7) | 2 (14.3) | 7 (43.8) | 1 (14.3) | 2 (33.3) | |
| Multiple regional | 1 (6.7) | 3 (21.4) | 3 (18.8) | 2 (28.6) | 1 (16.7) | |
| Diffuse | 1 (6.7) | 4 (28.6) | 1 (6.3) | 0 (0) | 0 (0) | |
| Internal enhancement | | | | | | |
| Heterogeneous | 14 (93.3) | 12 (85.7) | 15 (93.8) | 4 (57.1) | 4 (66.7) | 0.071 |
| Clumped | 1 (6.7) | 0 (0) | 1 (6.3) | 1 (14.3) | 1 (16.7) | |
| Clustered ring | 0 (0) | 2 (14.3) | 0 (0) | 2 (28.6) | 1 (16.7) | |
| Intratumoral signal intensity on T2w | | | | | | |
| Low/equal | 23 (85.2) | 30 (83.3) | 32 (94.1) | 15 (88.2) | 12 (60.0) | 0.037 |
| High | 4 (14.8) | 6 (16.7) | 2 (5.9) | 2 (11.8) | 8 (40.0) | |
| Kinetic curve pattern | | | | | | |
| Persistent | 9 (33.3) | 9 (25.0) | 9 (26.5) | 7 (41.2) | 4 (20.0) | 0.337 |
| Plateau | 2 (7.4) | 7 (19.4) | 8 (23.5) | 1 (5.9) | 7 (35.0) | |
| Washout | 16 (59.3) | 20 (55.6) | 17 (50.0) | 9 (52.9) | 9 (45.0) | |

Data are numbers with percentages in parentheses. Percentages may not add up to 100% because of rounding

*IDC* invasive ductal carcinoma, *HER2* human epidermal growth factor receptor 2, *T2w* T2-weighted imaging

to that of mean $ADC_{800}$ (0.782 vs. 0.780, $p = 0.97$). By using mean $ADC_{1500}$ for the differential diagnosis, the sensitivity and specificity were 70.6% and 69.2%, respectively.

Results of univariate and multivariate logistic regression analyses are summarized in Tables S1-S5 in the Supplemental Material 2. In the univariate regression analysis, $ADC_{1500}$ entropy (odds ratio [OR], 0.112; $p = 0.002$) was the only variable associated with luminal A, irregular mass shape (OR, 12.000; $p = 0.019$) and $ADC_{1500}$ entropy (OR, 4.642; $p = 0.020$) were associated with luminal B (HER2 positive), mean $ADC_{1500}$ (OR, 1884.897; $p = 0.018$) was the only variable associated with HER2 positive, and round/oval mass shape (OR, 3.529; $p = 0.039$), smooth mass margin (OR, 8.250; $p = 0.007$), rim enhancement (OR, 7.833; $p = 0.002$), and high intratumoral signal intensity on T2-weighted images (OR, 5.893; $p = 0.008$) were associated with triple negative. In the multivariate regression analysis, irregular mass shape (OR, 12.733; $p = 0.018$) and $ADC_{1500}$ entropy (OR, 4.557; $p = 0.022$) were associated with luminal B (HER2 positive), and smooth mass margin (OR, 9.129; $p = 0.012$) and rim enhancement (OR, 8.328; $p = 0.003$) were associated with triple negative.

**Table 3** ROC results of ADC parameters for IDC phenotype discrimination

| Parameters | Area under the ROC curve* | Threshold | Sensitivity† | Specificity† |
|---|---|---|---|---|
| Luminal A vs. other phenotypes | | | | |
| $ADC_{800}$ entropy | 0.818 (0.742, 0.879) | ≤ 5.40 | 74.1% (20/27) | 73.8% (79/107) |
| $ADC_{1500}$ entropy | 0.830 (0.756, 0.889) | ≤ 5.24 | 74.1% (20/27) | 76.6% (82/107) |
| HER2 positive vs. other phenotypes | | | | |
| Mean $ADC_{800}$ | 0.780 (0.701, 0.847) | > $0.94 \times 10^{-3}$ $mm^2/s$ | 70.6% (12/17) | 69.2% (81/117) |
| Mean $ADC_{1500}$ | 0.782 (0.702, 0.848) | > $0.74 \times 10^{-3}$ $mm^2/s$ | 70.6% (12/17) | 69.2% (81/117) |

*ROC* receiver-operating characteristic, *ADC* apparent diffusion coefficient, *IDC* invasive ductal carcinoma, *HER2* human epidermal growth factor receptor 2

* Data in parentheses are 95% confidence intervals

† Data in parentheses are numbers used to calculate percentages

## Discussion

Our results showed that mean tumor ADC values were associated with ER, PR, and HER2 expression statuses, while ADC entropy values were indicators of ER and Ki-67 in IDC. Among histologic phenotypes, luminal A subtype tended to display a lower ADC entropy value than other subtypes, while the HER2-positive subtype tended to display a higher mean ADC value. ADC metrics added value to conventional morphologic features in IDC phenotyping. In addition, ADC entropy derived from a high *b*-value (1500 s/$mm^2$) provided superior diagnostic performance compared with that from the standard *b*-value (800 s/$mm^2$) though the difference was not substantial for mean ADC.

ER and PR are hormone receptors known to be important prognostic factors and predictive biomarkers for response to endocrine therapy in breast cancer. In the present study, ER-/PR-positive tumors demonstrated substantially decreased mean ADC values compared with ER-/PR-negative tumors, and these results are in concordance with the findings of previous reports [6, 8, 9, 21]. Some studies suggested that ER expression is associated with inhibition of angiogenesis, which would reduce perfusion [22], as well as increased cellularity, which would restrict water diffusion [23]. Low vascularity and high cellularity could both contribute to decreased mean ADC values in ER-positive tumors. PR has generally been regarded as a marker of a functional ER pathway as transcription of the PR gene is enhanced and maintained by estrogens [24]. Therefore, PR-positive tumors also represented decreased mean ADC values, similar to ER-positive tumors.

HER2-overexpressing breast cancer exhibits increased cell proliferation and angiogenesis, associated with metastatic progression and poor prognosis [25]. Since high cellularity leads to restricted diffusion while high angiogenesis leads to increased diffusion, mean ADC values may be influenced in the opposite ways. In our study, high angiogenesis might play a dominant role over high cellularity, thus potentially causing increased mean ADC values in HER2-positive tumors. This result was consistent with the findings of previous studies [6, 7]. However, there were still several studies that found no relationship between HER2 expression status and mean ADC values, indicating that the effects of cellularity and vascularity on ADC might cancel out each other in their study subjects.

Ki-67 is a biologic marker considered to represent tumor proliferation status, with higher Ki-67 indices being associated with adverse clinical outcomes in patients with breast cancer [26]. It is likely that tumors with a high proliferation rate indicated by high Ki-67 would have increased cellularity. In our study, however, mean ADC values showed no substantial difference between high-proliferation (Ki-67 ≥ 20%) and low-proliferation (Ki-67 < 20%) groups, in accordance with the results of quite a few studies [6, 8, 21, 27, 28]. Additionally, a recently published meta-analysis reported an only weak correlation ($r$ = -0.22) between mean ADC values and Ki-67 in breast cancer and suggested that mean ADC could not be used as an imaging marker for Ki-67 [29]. Our results showed significant associations between ADC entropy values and Ki-67. Tumors with Ki-67 ≥ 20% exhibited increased ADC entropy values compared with those with Ki-67 < 20%. One possible explanation for these findings might be that high-proliferation tumors are more heterogeneous, characterized by complex changes including mitosis, angiogenesis, and necrosis. Mean ADC values are calculated by averaging ADC values of all pixels within ROIs and thus could not reflect the heterogeneity of breast cancer. However, ADC entropy represents the distribution of individual ADC values over all possible intensities and increases as the structure becomes more heterogeneous [17]. Therefore, ADC entropy might be superior to mean ADC for predicting Ki-67 status in breast cancer.

Luminal A breast cancer is defined as a low-proliferation subtype (low Ki-67) and generally has a favorable prognosis compared with other subtypes [2, 30]. Therefore, luminal A subtype showed the lowest ADC entropy values indicative of less intratumoral heterogeneity on ADC maps. Univariate logistic regression analysis showed that ADC entropy was the only variable associated with luminal A subtype. Among all subtypes, HER2-positive subtype showed the highest mean ADC values, which was also an independent risk factor at univariate logistic regression analysis. No significant difference in mean ADC values at either *b*-value was observed between HER2-positive and triple-negative subtypes. These findings agreed with results from the study by Martincich et al [8]. HER2-positive and triple-negative subtypes are associated with an aggressive course and poor prognosis compared with luminal subtype [30]. Martincich et al suggested that these more aggressive breast cancer subgroups are often characterized by benign imaging features instead, including high mean ADC values [8]. It has been reported that triple-negative breast cancer tends to have a round/oval mass shape, smooth mass margin, rim enhancement, and high intratumoral signal intensity on T2-weighted images [15, 31]. In the present study, two of those previously reported typical features including a smooth mass margin and rim enhancement were confirmed as independent predictors of triple-negative subtype. Multivariate logistic regression analysis also showed that irregular mass shape and ADC entropy were related to luminal B (HER2-positive) subtype. As luminal B (HER2-positive) subtype is both ER-/PR positive with lower ADC values and HER2 positive with higher ADC values, these contrary effects seem to cause the large ADC distribution heterogeneity in mass lesions. These findings suggested the utility of MR imaging in characterization of IDC histologic phenotypes, which might help in selecting the optimal treatment strategy and predicting prognosis and response to therapy.

Many previous studies have shown the potential of ADC maps obtained from standard *b*-value DWI (e.g., 800–1000 s/mm$^2$) in predicting molecular marker statuses and discriminating phenotypes of breast cancer. Our study further demonstrated that $ADC_{1500}$ outperformed $ADC_{800}$ in its accuracy and predictive power in terms of entropy values, which has rarely been reported to the best of our knowledge. In several studies comparing DWI obtained with standard and high *b*-values for breast cancer detection, a high *b*-value of 1500 s/mm$^2$ also showed better performance [32, 33]. We used a high *b*-value of 1500 s/mm$^2$ instead of a higher *b*-value because an insufficient signal-to-noise ratio and increased anatomical distortions at higher *b*-values would limit its clinical utility. In our study, mean ADC values decreased when the *b*-value increased from 800 to 1500 s/mm$^2$, which may be due to the biexponential DWI signal intensity attenuation in breast cancer [5, 27].

This study has several limitations. First, it was a retrospective study, and patient selection bias may potentially exist. Although we initially included all consecutive patients with breast malignancies at biopsy, still a large portion of them were excluded mainly because of consistency in histologic types and MR imaging settings. Moreover, the exclusion of patients with tumors difficult to identify or influenced by severe motion artifacts on DWI may also cause bias. This is mostly attributed to the inherent limitation of the single-shot spin-echo echo-planar imaging sequence, which has relatively low spatial resolution and high sensitivity to motion. Second, direct comparisons between ADC metrics and histopathologic factors such as cell density and microvessel density were lacking. Therefore, the explanation for the relationship between ADC metrics and molecular marker statuses was merely based on current findings from literature. Third, specimens for pathology did not necessarily match to the sites of sampling on ADC maps, although we used whole-tumor-based analysis. Fourth, a unified imaging protocol on the same MR imaging platform was performed. Further studies are needed to determine whether and to what degree the results may vary between different imagers, vendors, field strengths, and imaging parameters.

In conclusion, mean and entropy of ADC values provided complementary information and added value to conventional morphologic features to discriminate IDC phenotypes. In particular, mean ADC values were associated with ER, PR, and HER2 status, and ADC entropy values were associated with ER and Ki-67 status. Luminal A subtype showed lower ADC entropy values, and HER2-positive subtype showed higher mean ADC values. High-*b*-value $ADC_{1500}$ metrics may facilitate better phenotype discrimination than standard-*b*-value $ADC_{800}$ metrics.

**Funding** This study has received funding from the National Natural Science Foundation of China (nos. 81501458 and 81701642) and Medical Engineering Cross Research Foundation of Shanghai Jiao Tong University (nos. YG2015QN37 and YG2014ZD05).

## Compliance with Ethical Standards

**Guarantor** The scientific guarantor of this publication is Jianrong Xu.

**Conflict of Interest** The authors of this manuscript declare no relationships with any companies, whose products or services may be related to the subject matter of the article.

**Statistics and Biometry** No complex statistical methods were necessary for this paper.

**Informed Consent** Written informed consent was waived by the Institutional Review Board.

**Ethical Approval** Institutional Review Board approval was obtained.

**Study subjects or cohorts overlap** Some study subjects or cohorts have been previously reported in:

Suo S, Cheng F, Cao M et al (2017) Multiparametric diffusion-weighted imaging in breast lesions: Association with pathologic diagnosis and prognostic factors. J Magn Reson Imaging. DOI: 10.1002/jmri.25612

**Methodology**
- retrospective
- diagnostic or prognostic study
- performed at one institution

## References


1. Lam SW, Jimenez CR, Boven E (2014) Breast cancer classification by proteomic technologies: current state of knowledge. Cancer Treat Rev 40:129–138
2. Goldhirsch A, Winer EP, Coates AS et al (2013) Personalizing the treatment of women with early breast cancer: highlights of the St Gallen International Expert Consensus on the Primary Therapy of Early Breast Cancer 2013. Ann Oncol 24:2206–2223
3. Marusyk A, Polyak K (2010) Tumor heterogeneity: causes and consequences. Biochim Biophys Acta 1805:105–117
4. O'Connor JP, Rose CJ, Waterton JC, Carano RA, Parker GJ, Jackson A (2015) Imaging intratumor heterogeneity: role in therapy response, resistance, and clinical outcome. Clin Cancer Res 21:249–257
5. Catalano OA, Horn GL, Signore A et al (2017) PET/MR in invasive ductal breast cancer: correlation between imaging markers and histological phenotype. Br J Cancer 116:893–902
6. Jeh SK, Kim SH, Kim HS et al (2011) Correlation of the apparent diffusion coefficient value and dynamic magnetic resonance imaging findings with prognostic factors in invasive ductal carcinoma. J Magn Reson Imaging 33:102–109
7. Kim EJ, Kim SH, Park GE et al (2015) Histogram analysis of apparent diffusion coefficient at 3.0t: Correlation with prognostic factors and subtypes of invasive ductal carcinoma. J Magn Reson Imaging 42:1666–1678
8. Martincich L, Deantoni V, Bertotto I et al (2012) Correlations between diffusion-weighted imaging and breast cancer biomarkers. Eur Radiol 22:1519–1528
9. Guvenc I, Akay S, Ince S et al (2016) Apparent diffusion coefficient value in invasive ductal carcinoma at 3.0 Tesla: is it correlated with prognostic factors? Br J Radiol 89:20150614
10. Karan B, Pourbagher A, Torun N (2016) Diffusion-weighted imaging and (18) F-fluorodeoxyglucose positron emission tomography/computed tomography in breast cancer: Correlation of the apparent diffusion coefficient and maximum standardized uptake values with prognostic factors. J Magn Reson Imaging 43:1434–1444
11. Just N (2014) Improving tumour heterogeneity MRI assessment with histograms. Br J Cancer 111:2205–2213
12. Suo S, Zhang K, Cao M et al (2016) Characterization of breast masses as benign or malignant at 3.0T MRI with whole-lesion histogram analysis of the apparent diffusion coefficient. J Magn Reson Imaging 43:894–902
13. Shin HJ, Kim SH, Lee HJ et al (2016) Tumor apparent diffusion coefficient as an imaging biomarker to predict tumor aggressiveness in patients with estrogen-receptor-positive breast cancer. NMR Biomed 29:1070–1078
14. American College of Radiology (2013) Breast Imaging Reporting and Data System (BI-RADS), 5th edn. American College of Radiology, Reston, VA
15. Uematsu T, Kasami M, Yuen S (2009) Triple-negative breast cancer: correlation between MR imaging and pathologic findings. Radiology 250:638–647
16. Arponen O, Masarwah A, Sutela A et al (2016) Incidentally detected enhancing lesions found in breast MRI: analysis of apparent diffusion coefficient and T2 signal intensity significantly improves specificity. Eur Radiol 26:4361–4370
17. Fujimoto K, Tonan T, Azuma S et al (2011) Evaluation of the mean and entropy of apparent diffusion coefficient values in chronic hepatitis C: correlation with pathologic fibrosis stage and inflammatory activity grade. Radiology 258:739–748
18. Kim JH, Ko ES, Lim Y et al (2017) Breast Cancer Heterogeneity: MR Imaging Texture Analysis and Survival Outcomes. Radiology 282:665–675
19. Bustreo S, Osella-Abate S, Cassoni P et al (2016) Optimal Ki67 cut-off for luminal breast cancer prognostic evaluation: a large case series study with a long-term follow-up. Breast Cancer Res Treat 157:363–371
20. DeLong ER, DeLong DM, Clarke-Pearson DL (1988) Comparing the areas under two or more correlated receiver operating characteristic curves: a nonparametric approach. Biometrics 44:837–845
21. Iima M, Kataoka M, Kanao S et al (2018) Intravoxel incoherent motion and quantitative non-Gaussian diffusion MR imaging: evaluation of the diagnostic and prognostic value of several markers of malignant and benign breast lesions. Radiology 287:432–441
22. Ludovini V, Sidoni A, Pistola L et al (2003) Evaluation of the prognostic role of vascular endothelial growth factor and microvessel density in stages I and II breast cancer patients. Breast Cancer Res Treat 81:159–168
23. Jarque F, Lluch A, Vera FJ et al (1990) Intratumoral variation of estrogen and progesterone receptors in breast cancer: relationship with histopathological characteristics of the tumor. Oncology 47:9–13
24. Järvinen TA, Pelto-Huikko M, Holli K, Isola J (2000) Estrogen receptor beta is coexpressed with ERalpha and PR and associated with nodal status, grade, and proliferation rate in breast cancer. Am J Pathol 156:29–35
25. Vazquez-Martin A, Colomer R, Menendez JA (2007) Protein array technology to detect HER2 (erbB-2)-induced 'cytokine signature' in breast cancer. Eur J Cancer 43:1117–1124
26. Kontzoglou K, Palla V, Karaolanis G et al (2013) Correlation between Ki67 and breast cancer prognosis. Oncology 84:219–225
27. Suo S, Cheng F, Cao M et al (2017) Multiparametric diffusion-weighted imaging in breast lesions: Association with pathologic diagnosis and prognostic factors. J Magn Reson Imaging 46:740–750
28. Lee HS, Kim SH, Kang BJ, Baek JE, Song BJ (2016) Perfusion parameters in dynamic contrast-enhanced MRI and apparent diffusion coefficient value in diffusion-weighted MRI: association with prognostic factors in breast cancer. Acad Radiol 23:446–456
29. Surov A, Meyer HJ, Wienke A (2017) Associations between apparent diffusion coefficient (ADC) and KI 67 in different tumors: a meta-analysis. Part 1: ADCmean. Oncotarget 8:75434–75444
30. Parker JS, Mullins M, Cheang MC et al (2009) Supervised risk predictor of breast cancer based on intrinsic subtypes. J Clin Oncol 27:1160–1167
31. Youk JH, Son EJ, Chung J, Kim JA, Kim EK (2012) Triple-negative invasive breast cancer on dynamic contrast-enhanced and diffusion-weighted MR imaging: comparison with other breast cancer subtypes. Eur Radiol 22:1724–1734
32. Takanaga M, Hayashi N, Miyati T et al (2012) Influence of b value on the measurement of contrast and apparent diffusion coefficient in 3.0 Tesla breast magnetic resonance imaging. Nihon Hoshasen Gijutsu Gakkai Zasshi 68:201–208
33. Tamura T, Murakami S, Naito K, Yamada T, Fujimoto T, Kikkawa T (2014) Investigation of the optimal b-value to detect breast tumors with diffusion weighted imaging by 1.5-T MRI. Cancer Imaging 14:11